Eur. Phys. J. D (2018) 72: 27
https://doi.org/10.1140/epjd/e2017-80479-8

THE EUROPEAN PHYSICAL JOURNAL D

Regular Article

Collision cross sections and transport coefficients of O^-, O_2^-, O_3^- and O_4^- negative ions in O_2, N_2 and dry air for non-thermal plasmas modelling

Ali Hennad[1,a] and Mohammed Yousfi[2]

[1] Université des Sciences et de la Technologie d'Oran Mohamed Boudiaf, USTO-MB, FGE-LMSE, BP 1505 El M'Naouer, 31000 Oran, Algeria
[2] Université de Toulouse, Laplace UMR 5213 CNRS, UPS, 118 Route de Narbonne, 31062 Toulouse Cedex 9, France

Received 19 July 2017 / Received in final form 23 November 2017
Published online 6 February 2018 –

Abstract. The ions interaction data such as interaction potential parameters, elastic and inelastic collision cross sections and the transport coefficients (reduced mobility and diffusion coefficients) have been determined and analyzed in the case of the main negative oxygen ions (O^-, O_2^-, O_3^- and O_4^-) present in low temperature plasma at atmospheric pressure when colliding O_2, N_2 and dry air. The ion transport has been determined from an optimized Monte Carlo simulation using calculated elastic and experimentally fitted inelastic collision cross sections. The elastic momentum transfer collision cross sections have been calculated from a semi-classical JWKB approximation based on a $(n-4)$ rigid core interaction potential model. The cross sections sets involving elastic and inelastic processes were then validated using measured reduced mobility data and also diffusion coefficient whenever available in the literature. From the sets of elastic and inelastic collision cross sections thus obtained for the first time for O_3^-/O_2, O_2^-/N_2, O_3^-/N_2, and O_4^-/N_2 systems, the ion transport coefficients were calculated in pure gases and dry air over a wide range of the density reduced electric field E/N.

1 Introduction

In the case of low temperature plasmas generated in air at atmospheric pressure under corona or dielectric barrier electrode configuration, it is known that charged particles play an important role in the discharge dynamics and the associated chemical reaction kinetics. The better knowledge of spatio-temporal evolution of charged particles and neutral reactive oxygen and nitrogen species is very useful in many applications (in for instance plasma medicine see e.g. [1] or plasma pollution control of air see e.g. [2]). To obtain such plasma characteristics, in addition to the various diagnostic techniques, we particularly need the development of complex models of streamer dynamics coupled to plasma chemistry models [2]. As underlined elsewhere [3] such models require an a priori knowledge of many input basic data more particularly those involving the electron impacts with air molecules which are generally known enough and also those corresponding to the ion interactions. In the case of the ion transport in dry air, previous works (see e.g. [4]) have already given the basic data of several positive ions in air plasmas but there are in the literature only a few collision and transport data of negative oxygen ions in O_2, N_2, and dry air plasmas. The present paper is devoted to the collection and the determination of basic data (collision cross sections and transport coefficients) of several negative ions generated in dry air plasma either by dissociation of molecular oxygen or water vapor present in air as atomic ion O^- or by three body attachment as diatomic ion O_2^-, or the polyatomic ions O_3^- and O_4^- present in ambient air discharges mainly at high pressure. Indeed, if the monoatomic O^- ion is generally the most abundant negative ion in low pressure air plasmas, the molecular polyatomic ions (O_2^-, O_3^- and O_4^-) become the dominant negative ions in atmospheric pressure non-equilibrium discharges. These polyatomic ions have a non-negligible contribution in the space charge development and also in the ion chemistry as it can been seen in some works on modelling of the chemical kinetics in for instance plasma jets propagating in ambient air (see e.g. [5,6]). Furthermore, it would be important to note that the need for such data has been stressed very clearly in some review roadmaps (see for instance [7]). In addition data presented here would be invaluable in data bases such as QDB [8]. Noting that the reader can find some useful information about negative ions and also positive ions reactions with molecules in the Franklin textbook [9] while there are interesting information on the methodology of the determination of cross sections and transport properties of some negative ions [10] or positive ions [11,12] in atomic or molecular gases.

[a] e-mail: ali_hennad@yahoo.fr

Table 1. Energy of potential well ε_m, position of potential minimum r_m, and exponent n of the interaction potentials for the systems O^-, O_2^-, O_3^- and O_4^- ions in O_2 and N_2 respectively.

	ε_m (meV)	r_m (Å)	n
O^-/O_2	180.96	2.637	6
O_2^-/O_2	345.54	1.987	12
O_3^-/O_2	84.880	3.311	6
O_4^-/O_2	34.470	4.843	6
O^-/N_2	193.89	2.525	6
O_2^-/N_2	140.46	2.963	6
O_3^-/N_2	81.860	3.513	6
O_4^-/N_2	56.010	4.574	6

The calculation method of elastic momentum transfer cross section based on a JWKB approximation using a rigid core interaction potential model is described in Section 2 with the elastic momentum collision cross section giving the best fit with the measured ions transport coefficients. The latter have been obtained from an optimized Monte Carlo method [13]. The other ion data (inelastic collisions and transport coefficients) for the considered oxygen negative ions (O^-, O_2^-, O_3^- and O_4^-) are given in Section 3 for interactions with O_2, Section 4 for interactions with N_2 and Section 5 for interactions with air.

2 Method of calculation and elastic collision cross sections

The ion transport and reaction coefficients are calculated from an optimized Monte Carlo method well adapted to both symmetric and asymmetric ion/gas system [13]. This needs as input data both elastic and inelastic collision cross sections. The elastic momentum transfer cross section has been calculated using a semi-classical formalism based on the JWKB approximation for the phase shift using a rigid core potential model describing the ion/molecule interaction [14]:

$$V(r) = \frac{n\varepsilon_m}{3n-12}\left\{\frac{12}{n}\left(\frac{r_m-a}{r-a}\right)^n - 3\left(\frac{r_m-a}{r-a}\right)^4\right\}, \quad (1)$$

where r is the intermolecular distance, ε_m is the minimum energy of the potential, r_m is the position of the minimum, n is the power of the repulsive part of the potential and a is the shift between the mass and the charge centers. Following previous works (see e.g. [15–18]), exponent n is equal either $n = 12$ in the case of symmetric system (ion colliding parent gas) or $n = 6$ in the case of asymmetric system (ion colliding non parent gas). From the potential parameters neutral-neutral systems (see e.g. [19–21]), the potential parameters of equation (1) are given in Table 1 for the collision systems O^-/O_2, O_2^-/O_2, O_3^-/O_2, O_4^-/O_2, O^-/N_2, O_2^-/N_2, O_3^-/N_2, and O_4^-/N_2 while their associated interaction potentials are plotted in Figure 1. It is noteworthy that for the present asymmetric systems (O^-/O_2, O_3^-/O_2, O_4^-/O_2, O^-/N_2, O_2^-/N_2, O_3^-/N_2, and O_4^-/N_2), and symmetric systems (O_2^-/O_2), the best fit of the potential parameters has obtained from comparison with the measured ion transport parameters. Figure 1 shows the three classical regions in the potential variation. The first one is relative to the short internuclear distance range corresponding to the high energy region where there the interaction potential is dominated by nuclear repulsion. This is followed by an intermediate energy region where the electrostatic forces of both the nuclear repulsion and the attraction forces between the ion and the dipole moment induced on the neutral are present. The third region is the lower energy range, corresponding to long internuclear distance where attraction forces are predominant.

In the framework of the JWKB approximation, the phase shift δ_l depends on the impact parameter b and

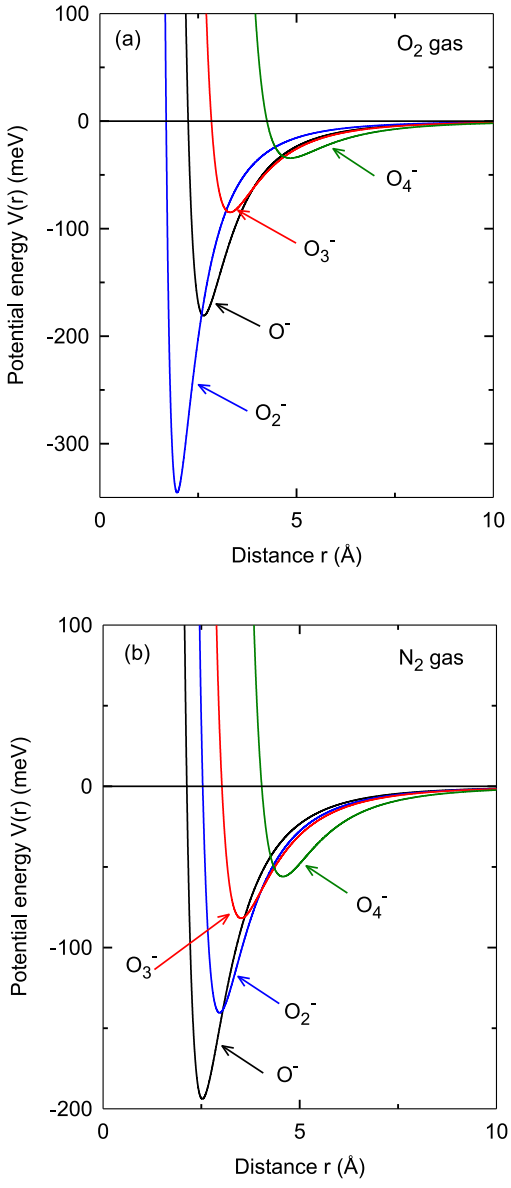

Fig. 1. Interaction potentials for O^-, O_2^-, O_3^- and O_4^- negative ions in (a) O_2 and (b) N_2.

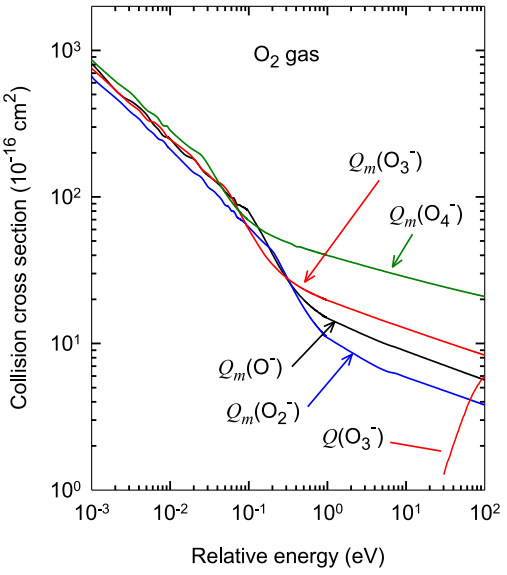

Fig. 2. Elastic momentum transfer collision cross sections Q_m as a function of the relative ion energy for O^-/O_2, O_2^-/O_2, O_3^-/O_2, and O_4^-/O_2 collisional systems.

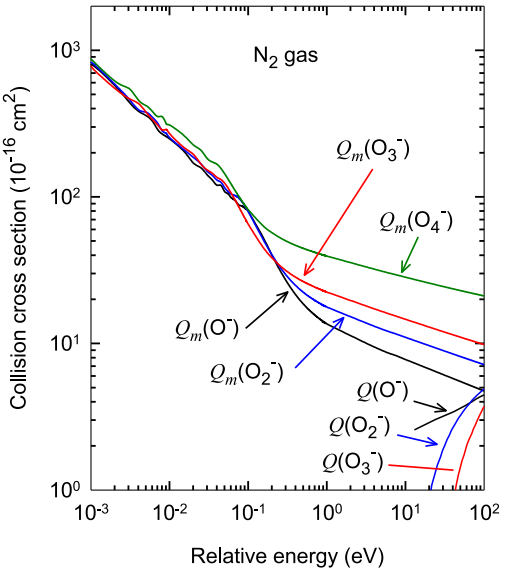

Fig. 3. Elastic momentum transfer collision cross sections Q_m as a function of the relative ion energy for O^-/N_2, O_2^-/N_2, O_3^-/N_2, and O_4^-/N_2 collisional systems.

interaction potential $V(r)$ as follows [14]:

$$\delta_l \approx \delta(b) = k\int_{r_c}^{\infty}\left(1-\frac{b^2}{r^2}-\frac{V(r)}{\varepsilon_r}\right)^{1/2}dr - k\int_{b}^{\infty}\left(1-\frac{b^2}{r^2}\right)^{1/2}dr, \quad (2)$$

with $b = (l+1/2)/k$, where l is the angular momentum quantum number, b the impact parameter and k the wave number of the relative motion proportional to the ion/molecule relative energy ε_r. The elastic momentum transfers cross section $Q_m(\varepsilon_r)$ is then calculated from:

$$Q_m(\varepsilon_r) = \frac{4\pi}{k^2}\sum_{l=0}^{\infty}(l+1)\sin^2(\delta_{l+1}-\delta_l). \quad (3)$$

Figures 2 and 3 display an overview on the elastic momentum transfer cross sections Q_m determined from the previously described procedure in the case of the chosen O^-, O_2^-, O_3^- and O_4^- ions in O_2 and N_2. Elastic momentum transfers cross section data for O_3^-/O_2, O_2^-/N_2, O_3^-/N_2, and O_4^-/N_2 systems are not previously available and given in the present work for the first time in the literature.

The different energy cross section shapes can be directly related to the long-range potential in the low energy region and to short-range potential in the low energy region and to the short-range potential in the high energy region. In the intermediate energy range, corresponding more particularly to the mean ion energy range corresponding to streamer, corona, and dielectric barrier gas discharges, the collision cross sections which have specific shape depend both on the attractive and the repulsive branches of our considered potential (see relation (1)). More generally, a potential branch varying as r^{-n} leads to a momentum transfer cross section Q_m varying as $Q_m(\varepsilon_r)\alpha\varepsilon_r^{-2/n}$. This means that in the low energy range where polarization (i.e. $n = 4$) is dominant we have $Q_m(\varepsilon_r)\alpha\varepsilon_r^{-1/2}$, which is coherent with Langevin theory. This also means that in the high energy range where the repulsive branch is dominant, we have $Q_m(\varepsilon_r)\alpha\varepsilon_r^{-1/6}$ for the symmetric systems (i.e. O_2^-/O_2) and $Q_m(\varepsilon_r)\alpha\varepsilon_r^{-1/3}$ for the other considered asymmetric systems (i.e. O^-, O_3^-, O_4^- in O_2 and O^-, O_2^-, O_3^-, O_4^- in N_2).

The ions O^-, O_2^-, O_3^-, and O_4^- in O_2 and N_2 can undergo elastic and also inelastic collisions in the energy range up to about 100 eV needed for modelling of low temperature pressure discharges in air discharges. Elastic collisions Q_m are calculated from interaction potential as previously described while inelastic collisions in the present ion/molecule systems can be the ion conversions and negative ion electron detachment. Therefore, for each considered ion/molecule system, the chosen set of collision cross sections must necessarily involve both elastic and inelastic ion/molecule collisions in order to be representative of the transport and reactivity of the ion in a gas or a gas mixture such air under a given applied electric field. This is why in the following; we first give the different ion/gas processes occurring for each considered system. The associated inelastic collision cross sections are taken from literature compilation. The chosen set of collision cross sections is then fitted and validated using a classical swarm unfolding technique. This means that the chosen collision cross sections are used in an optimized placeMonte Carlo method for ion swarm data calculations. This allows the validation step from a comparison between the calculated swarm data and the available measured one until the best agreement is obtained. In the following, for each ion/gas system, we give the ion/molecule reactions

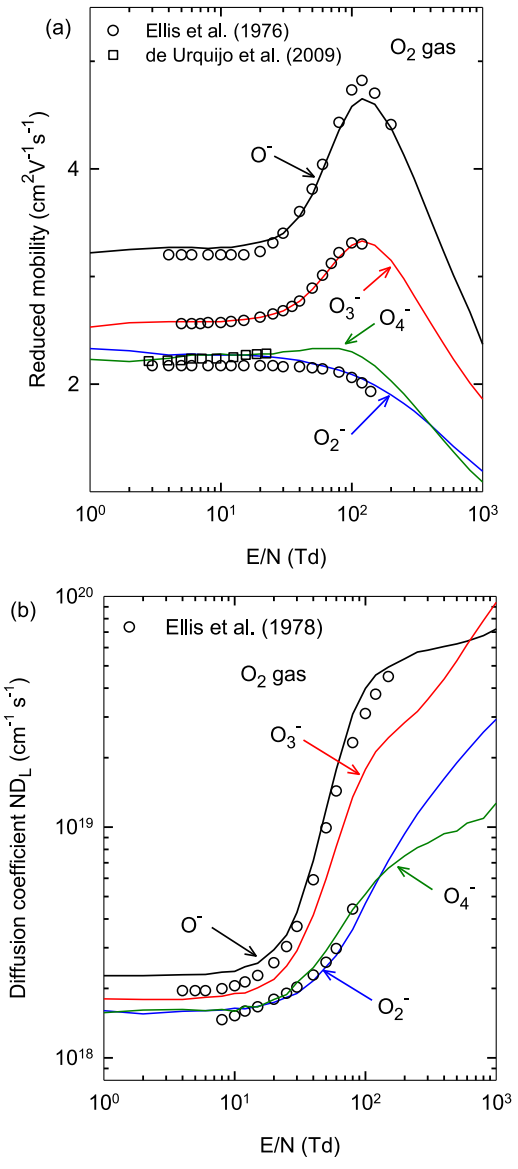

Fig. 4. (a) Ions mobility, (b) longitudinal diffusion coefficient calculated as a function of E/N for O^-/O_2, O_2^-/O_2, O_3^-/O_2, and O_4^-/O_2 systems using previous sets of collision cross sections.

and the associated inelastic collision cross sections. We also give ion swarm parameters when available in the literature. The fitted collision cross sections of the different ion/gas systems are given from 10^{-3} up to 100 eV in O_2, N_2, and dry air. Then, the calculated swarm parameters are given for a reduced field E/N varying from 1 up to 1000 Td using our Monte Carlo method [13].

3 Transport coefficients of negative oxygen ions in oxygen

The inelastic cross sections of O^-, O_2^-, and O_4^- ions in O_2 used in this work are given in literature by Benhenni et al. [22], Yousfi et al. [13], Hennad [23], Petrović et al. [24], and de Urquijo et al. [25] respectively. For O_3^-/O_2 system, in the energy range our interest, the most probable collision processes are:

$$O_3^- + O_2 \rightarrow O_3^- + O_2, \quad \text{(R1)}$$

$$O_3^- + O_2 \rightarrow \text{Products} + 4.75\,\text{eV}. \quad \text{(R2)}$$

Reaction (R1) is represented by the elastic momentum transfer cross section $Q_m(O_3^-)$ calculated from (6-4) core potential (see Fig. 2). The exothermic reaction (R2) is observed by Ranjan and Goodyear [26] without specifying the products for the reaction (R2). This cross section $Q(O_3^-)$ (see Fig. 2) of reaction (R2) is given by Ranjan and Goodyear [26]. This inelastic cross sections has a negligible influence on the calculation of ion transport coefficient in the energy range our interest.

The collision cross sections are chosen from the good agreement observed between the calculated O^-, O_2^-, O_3^-, and O_4^- ions mobility data in O_2 and the measured one (see e.g. [27–30]). Such good agreement is shown in Figure 4 displaying reduced mobility data and longitudinal diffusion coefficients of the four considered negative ions in O_2. According to Hennad [23], the mobility is known to be inversely proportional to elastic momentum transfer collision cross sections. We note that mobility of O_2^- in O_2 is the lowest compared of O^-, O_3^-, and O_4^- ions mobility in same gas, despite the low amplitude of the cross section $Q_m(O_2^-)$ (see Fig. 2). The system O_2^-/O_2 is a symmetric system which includes the presence of the resonant charge transfer cross section [23,31], which directly in O_2 fluences the magnitude of O_2^- mobility in O_2. In Figure 4b, we display the normalized longitudinal ND_L (longitudinal diffusion coefficient) in comparison with some available experimental [32] data for O^-, O_2^-, O_3^- and O_4^- ions in O_2 as function of E/N.

4 Transport coefficients of negative oxygen ions in nitrogen

In the energy range our interest, the most probable collision processes are:

$$A^- + N_2 \rightarrow A^- + N_2, \quad \text{(R3)}$$

$$O^- + N_2 \rightarrow N_2O + e^- + 0.2\text{eV}, \quad \text{(R4)}$$

$$O_2^- + N_2 \rightarrow \text{Products}, \quad \text{(R5)}$$

$$O_3^- + N_2 \rightarrow \text{Products}, \quad \text{(R6)}$$

Reaction (R3) represents the elastic collision for A^- negative ion (A^- being either O^-, or O_2^-, or O_3^-, or O_4^-) impacting N_2. The momentum transfer cross section $Q_m(A^-)$ calculated from (6-4) core potential is already displayed in Figure 3. The exothermic reaction (4) [33]

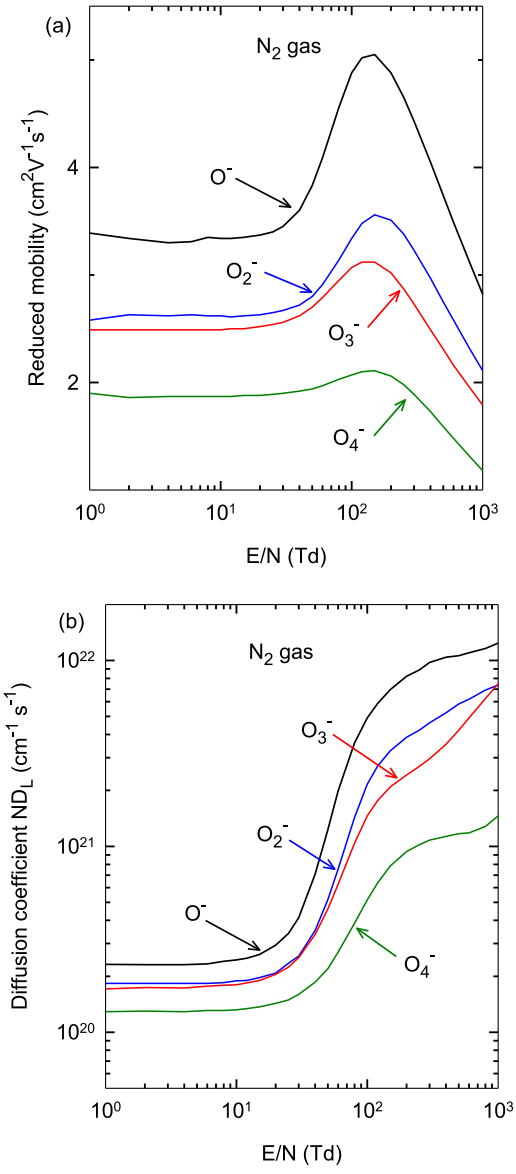

Fig. 5. (a) Ions mobility, (b) longitudinal diffusion coefficient calculated as a function of E/N for O^-/N_2, O_2^-/N_2, O_3^-/N_2, and O_4^-/N_2 systems using previous sets of collision cross sections.

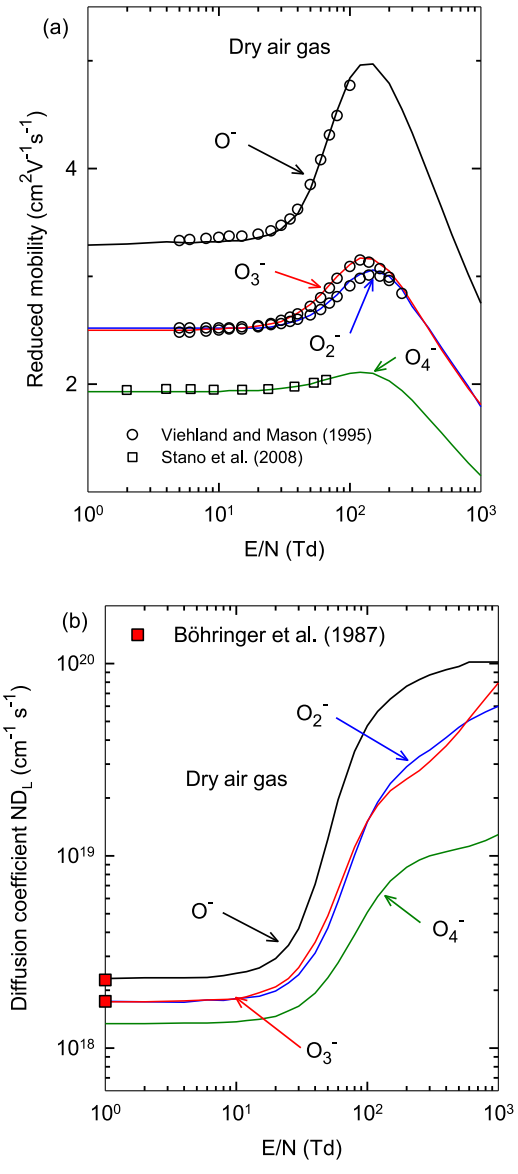

Fig. 6. (a) Ions mobility, (b) longitudinal diffusion coefficient calculated as a function of E/N of O^-, O_2^-, O_3^-, and O_4^- ions in dry air.

represents electron detachment producing N_2O molecule. The inelastic cross section $Q(O^-)$ shown in Figure 3 is given by Ranjan and Goodyear [26]. The collision cross sections of the two last reactions ((R5) and (R6)) are given in the same reference [26] which does not specified the nature of the products when O_2^- and O_3^- ions collide N_2 (reactions (R5) and (R6)). The inelastic cross sections $Q(O_2^-)$ and $Q(O_3^-)$ (see Fig. 3) corresponding to reactions (R5) and (R6) are taken from [26], while the set cross section of O^-/N_2 system is given in literature [22].

As there is no literature experimental transport data for these four negative ions in N_2, the calculations of their transport coefficients in O_2 are first based on the best fit with the experimental transport data of these ions in O_2 and dry air. The obtained reduced ion mobility data and the normalized longitudinal ND_L of these four considered negative oxygen ions (O^-, O_2^-, O_3^-, and O_4^-) in N_2 are displayed in Figure 5. Noting that these transport coefficients of the four negative oxygen ions in N_2 are given in the present work for the first time in the literature.

5 Transport coefficients of negative oxygen ions in dry air

For the simulation of charged particle dynamics in the case of non-thermal discharge in dray air at atmospheric pressure, it is necessary to know the charged particle data for a large range of E/N variation. As underlined in the introduction, the data of electrons and the main positive ions are already given in the literature while those of the

Table 2. O^-, O_2^-, O_3^- and O_4^- ion reduced mobility data K_0 in dry air.

E/N (Td)	K_o ($cm^2\,V^{-1}\,s^{-1}$)			
	O^-	O_2^-	O_3^-	O_4^-
1	3.30	2.52	2.50	1.93
2	3.30	2.52	2.50	1.93
4	3.30	2.52	2.50	1.93
6	3.31	2.52	2.50	1.93
8	3.32	2.52	2.51	1.93
10	3.32	2.52	2.51	1.93
12	3.33	2.52	2.52	1.94
15	3.33	2.52	2.52	1.94
20	3.36	2.52	2.54	1.94
25	3.39	2.53	2.56	1.95
30	3.44	2.55	2.58	1.96
40	3.58	2.59	2.66	1.98
50	3.81	2.64	2.74	2.00
60	4.08	2.70	2.83	2.03
80	4.54	2.83	3.00	2.07
100	4.84	2.96	3.11	2.10
120	4.96	3.02	3.17	2.11
150	4.97	3.06	3.16	2.10
200	4.79	3.00	3.05	2.03
250	4.55	2.88	2.90	1.94
300	4.33	2.72	2.75	1.85
400	3.94	2.52	2.51	1.68
500	3.64	2.34	2.32	1.55
600	3.39	2.20	2.18	1.44
800	3.02	1.98	1.96	1.27
1000	2.75	1.790	1.81	1.15

Table 3. Longitudinal diffusion coefficient ND_L data of O^-, O_2^-, O_3^- and O_4^- ions in dry air.

E/N (Td)	$ND_L(10^{19}\,cm^{-1}\,s^{-1})$			
	O^-	O_2^-	O_3^-	O_4^-
1	0.230	0.175	0.174	0.134
2	0.232	0.174	0.174	0.134
4	0.232	0.173	0.176	0.135
6	0.233	0.178	0.178	0.135
8	0.238	0.177	0.179	0.136
10	0.245	0.181	0.180	0.137
12	0.250	0.183	0.185	0.139
15	0.261	0.186	0.194	0.141
20	0.292	0.198	0.208	0.146
25	0.342	0.218	0.230	0.156
30	0.418	0.241	0.262	0.165
40	0.711	0.312	0.355	0.193
50	1.220	0.421	0.487	0.232
60	1.960	0.580	0.669	0.278
80	3.500	1.010	1.110	0.388
100	4.750	1.500	1.510	0.508
120	5.640	1.900	1.830	0.613
150	6.550	2.380	2.180	0.740
200	7.630	2.910	2.510	0.872
250	8.260	3.290	2.780	0.952
300	8.730	3.550	3.090	1.000
400	9.290	4.120	3.730	1.050
500	9.660	4.660	4.420	1.090
600	10.200	5.070	5.180	1.120
800	10.200	5.610	6.600	1.200
1000	10.200	6.000	7.930	1.290

negative oxygen ions (O^-, O_2^-, O_3^-, and O_4^-) are completed and determined in previous sections of the present work. Therefore, as soon as the sets of the elastic and inelastic collision cross sections are known for a given ion in each pure gas (i.e. O_2 or N_2), it is possible to calculate the corresponding ion transport coefficients in dry air. The ion swarm parameters (mainly mobility and diffusion coefficient) are calculated from our optimized Monte Carlo technique using the present sets of collision cross sections for the different ion/gas systems considered in this work, i.e. the ion/O_2 systems O^-/O_2, O_2^-/O_2, O_3^-/O_2, and O_4^-/O_2 and also the ion/N_2 systems O^-/N_2, O_2^-/N_2, O_3^-/N_2, and O_4^-/N_2. The mobility data of these ions O^-, O_2^-, O_3^-, and O_4^- in dry air display a plateau in the low reduced fields E/N range (see Fig. 6). This plateau is governed as previously stated by the polarization potential. This trend is followed by a maximum and then a monotonic decrease at higher reduced fields.

Figure 6 shows a good agreement between the calculated O^-, O_2^-, O_3^-, and O_4^- ions mobility data in dry air and those the literature measurements [34–36]. It is also given in Figure 6, the variation of longitudinal diffusion coefficients of these four negative ions in dry air for the first time in the literature over a large range of E/N. For finish, the Tables 2 and 3 give the numerical data of the ion mobility and longitudinal diffusion coefficient of negative ions (O^-, O_2^-, O_3^- and O_4^-) in dry air calculated from Monte Carlo method using the present sets of collision cross in this work.

6 Conclusion

In the case of the collision systems O_3^-/O_2, O_2^-/N_2, O_3^-/N_2, and O_4^-/N_2, the sets of collision cross sections are given for the first time in the literature from more particularly the fitting of the minimum of the potential energy well and the position of potential minimum of a $(n-4)$ core interaction potential. The corresponding mobility and longitudinal diffusion coefficient data are analysed and compared with experimental data in order to obtain the best fit of the corresponding elastic and inelastic collision cross sections. Thus, the transport data of these main negative ions can be therefore used as they are for the physical fluid modelling of charged particle dynamics in corona or dielectric barrier discharges in dry air at atmospheric pressures where more particularly such polyatomic negative oxygen ions can be the most abundant produced ions.

The first author (invited professor) would like to thank M. Yousfi (CNRS Professorship) for his invitation during one month in the PRHE team of the Laplace Laboratory of University of Toulouse.

Author contribution statement

The authors were contributed to the manuscript conception, preparation and writing with an equal proportion.

References

1. M. Yousfi, N. Merbahi, A. Pathak, O. Eichwald, Fundam. Clin. Pharmacol. **28**, 123 (2014)
2. O. Eichwald, M. Yousfi, A. Hennad, M.D. Benabdessadok, J. Appl. Phys. **82**, 4781 (1997)
3. M. Yousfi, A. Bekstein, N. Merbahi, O. Eichwald, O. Ducasse, M. Benhenni, J.P. Gardou, Plasma Sour. Sci. Technol. **19**, 034004 (2010)
4. A. Bekstein, M. Yousfi, M. Benhenni, O. Ducasse, O. Eichwald, J. Appl. Phys. **107**, 103308 (2010)
5. T. Murakami, K. Niemi, T. Gans, D. O'Connell, W.G Graham, Plasma Sour. Sci. Technol. **22**, 015003 (2013)
6. W. Van Gaens, A. Bogaerts, J. Phys. D: Appl. Phys. **46**, 275201 (2013)
7. P.J. Bruggeman, M.J. Kushner, B.R. Locke, J.G.E. Gardeniers, W.G. Graham, D.G. Graves, R.C.H.M. Hofman-Caris, D. Maric, J.P. Reid, E. Ceriani, D. Fernandez Rivas, J.E. Foster, S.C. Garrick, Y. Gorbanev, S. Hamaguchi, F. Iza, H. Jablonowski, E. Klimova, J. Kold, F. Krcma, P. Lukes, Z. Machala, I. Marinov, D. Mariotti, S. Mededovic Thagard, D. Minakata, E.C. Neyts, J. Pawlat, Z.Lj. Petrovic, R. Pflieger, S. Reuter, D.C. Schram, S. Schröter, M. Shiraiwa, B. Tarabova, P.A. Tsai, J.R.R. Verlet, T. von Woedtke, K.R. Wilson, K. Yasui, G. Zvereva, Plasma Sour. Sci. Technol. **25**, 053002 (2016)
8. J. Tennyson, S. Rahimi, C. Hill, L. Tse, A. Vibhakar, D. Akello-Egwel, D.B. Brown, A. Dzarasova, J.R. Hamilton, D. Jaksch, S. Mohr, K. Wren-Little, J. Bruckmeier, A. Agarwal, K. Bartschat, A. Bogaerts, J.-P. Booth, M.J. Goeckner, K. Hassouni, Y. Itikawa, B.J. Braams, E. Krishnakumar, A. Laricchiuta, N.J. Mason, S. Pandey, Z.Lj. Petrovic, Y.-K. Pu, A. Ranjan, S. Rauf, J. Schulze, M.M. Turner, P. Ventzek, J.C. Whitehead, J.-S. Yoon, Plasma Sour. Sci. Technol. **26**, 055014 (2017)
9. J.L. Franklin, in *Ion-molecule reactions*, edited by Department of Chemistry Rice University Houston, Texas (Plenum Press, New York, 1972)
10. V.J. Jovanovic, Z.Lj. Petrovic, J. Phys.: Conf. Ser. **162**, 012004 (2009)
11. A.V. Phelps, J. Chem. Phys. Ref. Data **20**, 557 (1991)
12. M.V.V.S. Rao, R.J. Van Brunt, J.K. Olthoff, Phys. Rev. E **59**, 4565 (1999)
13. M. Yousfi, A. Hennad, O. Eichwald, J. Appl. Phys. **84**, 107 (1998)
14. D. Nelson, M. Benhenni, M. Yousfi, O. Eichwald, J. Phys. D: Appl. Phys. **34**, 3247 (2001)
15. A. Hennad, M. Yousfi, J. Phys. D: Appl. Phys. **44**, 025201 (2011)
16. M. Yousfi, A. Hennad, M. Benhenni, J. Phys. D: Appl. Phys. **40**, 1751 (2007)
17. M. Yousfi, A. Hennad, M. Benhenni, O. Eichwald, N. Merbahi, J. Appl. Phys. **112**, 043301 (2012)
18. M. Benhenni, M. Yousfi, J. de Urquijo, A. Hennad, J. Phys. D: Appl. Phys. **42**, 125203 (2009)
19. M. Capitelli, C. Gorse, S. Longo, D. Giordano, J. Thermophys. Heat Transf. **14**, 259 (2000)
20. S. Bouazza, A. Barbe, J.J. Plateaux, L. Rosenmann, J.M. Hartmann, C. Camy-Peyret, J.M. Flaud, R.R. Gamache, J. Mol. Spectrosc. **157**, 271 (1993)
21. B. Brunetti, G. Liuti, E. Luzzatti, F. Pirani, F. Vecchiocattivi, J. Chem. Phys. **74**, 6734 (2016)
22. M. Benhenni, M. Yousfi, A. Bekstein, O. Eichwald, N. Merbahi, J. Phys. D: Appl. Phys. **39**, 4886 (2006)
23. A. Hennad, Ph.D thesis, Université Paul Sabatier, Toulouse, France No 2458, 1996
24. Z.Lj. Petrović, Z.M. Raspopović, V.D. Stojanović, J.V. Jovanović, G. Malović, T. Makabe, J. de Urquijo, Appl. Surf. Sci. **253**, 6619 (2007)
25. J. de Urquijo, A. Bekstein, O. Ducasse, G. Ruíz-Vargas, M. Yousfi, M. Benhenni, Eur. Phys. J. **55**, 637 (2009)
26. R. Ranjan, C.C. Goodyear, J. Phys. B: Atom. Mol. Phys. **6**, 1070 (1973)
27. H.W. Ellis, R.Y. Pai, E.W. McDaniel, E.A. Mason, L.A. Viehland, At. Data Nucl. Data Tables **17**, 177 (1976)
28. R.M. Snuggs, D.J. Volz, J.H. Schummers, D.W. Martin, E.W. McDaniel, Phys. Rev. A **3**, 477 (1971)
29. M.T. Elford, J.A. Rees, Aust. J. Phys. **27**, 333 (1974)
30. L.G. McKnight, Phys. Rev. A **2**, 762 (1970)
31. J.A. Rutherford, D.A. Vroom, J. Chem. Phys. **61**, 2514 (1974)
32. H.W. Ellis, E.W. McDaniel, D.L. Albritton, L.A. Viehland, S.L. Lin, E.A. Mason, At. Data Nucl. Data Tables **22**, 179 (1978)
33. E.E. Ferguson, F.C. Fehsenfeld, A.L. Schmeltekopf, *Chemical reactions in electrical discharges, Advances in chemistry*, edited by B. Blaustein (American Chemical Society, Washington, DC, 1969), pp. 83–91
34. L.A. Viehland, E.A. Mason, At. Data Nucl. Data Tables **60**, 37 (1995)
35. H. Böhringer, D.W. Fahey, W. Lindinger, F. Howorka, F.C. Fehsenfeld, D.L. Albritton, Int. J. Mass Spectrom. Ion Process. **81**, 45 (1987)
36. M. Stano, E. Safonov, M. Kučera, Š. Matejčik, Chem. Listy **102**, s1414 (2008)